Journal of Colloid and Interface Science 671 (2024) 457–468

Contents lists available at ScienceDirect

Journal of Colloid And Interface Science

journal homepage: www.elsevier.com/locate/jcis

Regular Article

Multifunctional photonic microobjects with asymmetric response in radial direction and their anticounterfeiting performance

Xiaoyang Du [a], Chengnian Li [b], Jianying Wang [c], Zhi Li [a], Jintao Zhu [b,*], Yajiang Yang [b], Yuandu Hu [a,d,*]

[a] Department of Materials Science and Engineering, School of Physical Science and Engineering, Beijing Jiaotong University, Beijing 100044, China
[b] Hubei Key Lab of Materials Chemistry and Service Failure, School of Chemistry and Chemical Engineering, Huazhong University of Science and Technology, Wuhan 430074, China
[c] Key Laboratory for the Green Preparation and Application of Functional Materials, Hubei Key Laboratory of Polymer Materials, Collaborative Innovation Center for Advanced Organic Chemical Materials Co-Constructed by the Province and Ministry of Education, School of Materials Science and Engineering, Hubei University, Wuhan 430062, China
[d] State Key Laboratory of Molecular Engineering of Polymers (Fudan University), Shanghai 200438, China

GRAPHICAL ABSTRACT

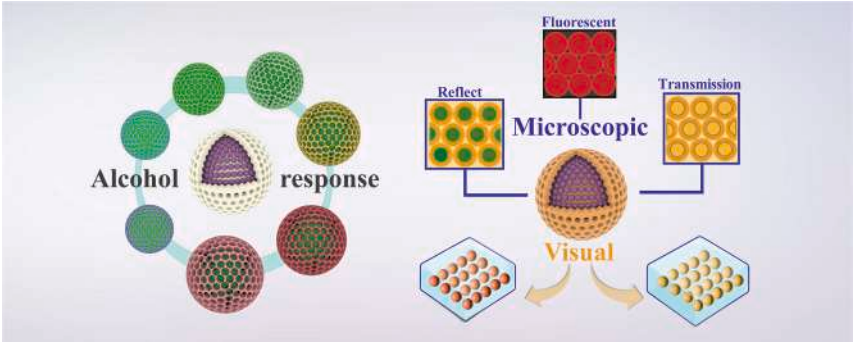

ARTICLE INFO

Keywords:
Photonic microobject
Hydrogels
Multiple colors
Stimulus-responsive property
Anticounterfeiting

ABSTRACT

There are few explorations that have integrated multiple properties into photonic microobjects in a facile and controlled manner. In this work, we present a straightforward method to integrate different functions into individual photonic microobject. Droplet-based microfluidics was used to produce uniform droplets of an aqueous dispersion of monodispersed SiO_2 nanoparticles (NPs). The droplets evolved into opal-structured photonic microballs upon complete evaporation of water. After infiltration of an aqueous solution of acrylamide (AAm) and acrylic acid (AAc) monomers into the interstices among SiO_2 NPs, opal-structured SiO_2 NPs/pAAm-*co*-AAc hydrogel composite photonic microballs were obtained upon UV irradiation. Afterwards, a wet etching process was introduced to etch the microballs in a controlled manner, yielding individual photonic microball composed of an SiO_2 NPs/pAAm-*co*-AAc composite opal core and a neat pAAm-*co*-AAc shell. The pendant carboxylic acid groups in the skeleton of the hydrogel matrix were further utilized to react with positively charged compounds, such as Ruthenium compound containing fluorescent polymers. The resulting photonic microobjects eventually

* Corresponding authors.
E-mail addresses: jtzhu@hust.edu.cn (J. Zhu), huyd@bjtu.edu.cn (Y. Hu).

https://doi.org/10.1016/j.jcis.2024.05.108
Received 8 February 2024; Received in revised form 26 April 2024; Accepted 15 May 2024
Available online 23 May 2024

featured with localized stimulus-responsive properties and multiple colors under different modes. The multi-functional photonic microobjects were discovered to have fivefold of anticounterfeiting properties when used as building blocks for anticounterfeiting structures and may have other potential applications.

1. Introduction

Structural colors have been widely found in our natural world, from tiny insects such as *Lamprocyphus augustus* to animals with relatively large body sizes, such as *Peacoks* and *Chameleons* [1,2].Many of those species could change their appearances over different time frames to adapt variations of ambient environment to camouflage [3].By leveraging this kind of fashion, the species could survive in the severe competition of our natural world. When their microstructures are filmed using modern instruments, such as electron microscopes, we are amazed by the exquisite and marvelous details, named as photonic structures that are based on the tiny ordered hierarchy structures and originated from numerous years of evolution and natural selection [4]. Human beings have been constantly acquiring knowledge from our nature to develop new materials that could advance our civilization [5]. Due to their wide applications, for decades, photonic structures have been among a category of materials having attracted a large amount of attention [6–14]. In particular, hydrogel photonic materials, such as hydrogel photonic microobjects, have been intensively investigated due to that they could interface materials science with a variety of other fields [15–18]. While the development of a single platform that could exceptionally integrate multiple functions, hydrogel photonic microobjects with a variety of forms have been designed and studied [19–22]. Microfluidics is a powerful platform that allows us to manipulate tiny amount of liquid for materials' designs and construction [23–28]. Self-assembly of colloids combined with microfluidics has been intensively used to generate different photonic microobjects, despite more expensive and sophisticated micro/nanofabrication technologies can also be used to produce photonic structures [29–33]. Depending on the internal structures of the photonic microobjects, opal and inverse-opal structures are the two common forms [18,34–39]. Normally, the resulting microobjects feature with a single stopband [31]. Although photonic microobjects with distinct stopbands can be obtained by physically merging or stacking of different photonic components, the resulting photonic microobjects either possess a Janus or multicompartmental configuration, leading their photonic properties to depend on orientations [19,40–45]. In light of this, photonic microobjects possess dual stopbands and beyond but with concentric configurations have been conceived and constructed by various strategies [24,46–49]. Nevertheless, majority of the resulting microobjects are lack of responsive property in a controlled manner, which is unfavorable to form complex structural colors in a hierarchy fashion. In addition, fluorescences are usually introduced into photonic microobjects by incorporating small molecular-based dyes or quantum dots (QDs) to integrate more functionalities [50,51]. However, those fluorescent components are either fail to preserve long-term fluorescent property with time increase or requiring complicated synthesis processes under strict conditions [52]. We herein prepared photonic microobjects composed of SiO_2 NPs and hydrogel skeleton, which could integrate both opal and inverse-opal structures into individual microobjects in a concentric configuration. The individual photonic microobject consists of a pAAm-*co*-AAc skeleton shell and a composite SiO_2 NPs/pAAm-*co*-AAc core. Subsequently, the negatively charged hydrogel skeleton pAAm-*co*-AAc can react with a positively charged Ruthenium-based compound, either a Ruthenium-based small molecule or Ruthenium-functionalized polymers simply by the electrostatic interaction. Eventually, the obtained microobjects possess multiple features, including dual stopbands, visible characteristic color from the Ruthenium moieties, localized stimulus-responsive property to ethanol and fluorescence property. The multiple features allow us to utilize the photonic microobjects for more further applications, such as building blocks of anticounterfeiting materials.

2. Experimental section/methods

2.1. Materials

Ammonia solution (≥28 % $NH_3{\cdot}H_2O$), Tetraethyl orthosilicate (TEOS, ≥ 98 %), anhydrous ethanol, 2, 2-diethoxy acetophenone (DEAP, >95 %), silicone oil (100 cSt.), acrylic acid, acrylamide (AAc, >99 %), N, N'-methylenebisacrylamide (99 %), poly(ethylene glycol)methyl ether methacrylate (OEGMA, Mn ~ 500), ethylene diacrylate (PEGDA, Mn ~ 600), Sodium alginate (SA, Mw = 20 000–50 000, viscosity = 15–60 mPa·s at 1 wt%), Calcium chloride-dihydrate ($CaCl_2{\cdot}2H_2O$, purity ≥99 %, Innochem Science and Technology Co., Beijing, China), poly (ethylene glycol) phenyl ether acrylate (PEGPEA, Mn ~ 324), methyl-fluorosilicone oil (ρ = 1.266 g/cm^3, viscosity 1000 cst at 25 °C, Xin' an Chemical Production), 4-vinyl-4′-methyl-2,2′-bipyridine, tris (2,2-Bipyridyl) Ruthenium (II) chloride hexahydrate, ammonium hexafluorophosphate (NH_4PF_6, ≥98.0 %), *n*-octadecyltrimethoxyl silane were purchased from Gelest, Inc. *N*-isopropyl acrylamide (NIPAAm, > 95 %) and deuterated DMSO (d^6-DMSO) were purchased from Sigma-Aldrich, China. Potassium persulfate (KPS, ≥99 %) was purchased from Aladdin. DC-749 silicone resin was ordered from Dow Corning, Inc. Ruthenium(4-vinyl-4′-methyl-2,2′-bipyridine)bis(2, 2′-bipyridine) bis (hexafluoro phosphate) was synthesized based on previous reports [53,54]. All other chemicals were purchased from Sigma-Aldrich and used as received.

2.2. Synthesis and purification of SiO_2 NPs

SiO_2 NPs were synthesized based on the hydrolysis reaction of tetraethyl orthosilicate (TEOS) according to the reported method [55]. Briefly, four different solutions were first prepared as follows: Solution A, a mixture of 5 mL ammonia solution and 22 mL ethanol. Solution B, a mixture of 0.8 mL TEOS and 22 mL ethanol. Solution C, 4 mL ammonia water. Solution D, a mixture of 1 mL TEOS and 44 mL ethanol. Four solutions were then mixed and reacted at the constant temperature (40 °C) for 6 h. After cooling down to the room temperature(~23 °C), the mixture solution was transferred to several 15 mL centrifuge tubes with equal amounts of solution, and centrifuged at 8000 rpm for 10 min. The precipitate was collected and re-dispersed with water. The centrifugation-redispersion process was repeated at least three times. Eventually, purified SiO_2 NPs were obtained.

2.3. Construction of microfluidic device for the preparation of single emulsion droplets

To obtain emulsion droplets with uniform size, a popularly-used microfluidic device was constructed and details for the construction of the device can be found in our previous reports [23,56]. The device consists of two round glass capillaries (inner diameter 580 μm, outer diameter 1 mm, from World Precision Instruments) and one square glass capillary (inner diameter 1 mm, from Vitrocom. Basically, a round glass capillary was pulled into two halves by a micro puller. The two halves were subsequently processed by a microforge instrument with orifices of 80 μm and ~300 μm, respectively. The capillary with a relatively larger orifice was used as the outlet collecting tube. To eliminate the wetting effect during the droplet production process, the round glass capillary with a 300 μm orifice was treated to hydrophobic with *n*-octadecyltrimethoxyl silane. The two tapered round capillaries were then

coaxially inserted into the square glass capillary. The coaxially assembled capillaries together with blunt syringe needles were then sealed by Devon 5-minute epoxy.

2.4. Preparation of spherical photonic crystal microobjects with opal structure using SiO_2 NPs as building blocks

The spherical photonic microobjects with opal structure were prepared by combining microfluidic emulsification with a subsequent solvent-evaporation process. In the microfluidic emulsification step, a silicone oil solution and an aqueous dispersion of SiO_2 NPs were used as continuous and dispersed phases, respectively. At optimal and stable flow rates, such as 200 μL/h (dispersed phase) and 3000 μL/h (continuous phase), single emulsions with a uniform size can be obtained. The droplet generation process was monitored and recorded using an upright optical microscope (LWD300-38LT, Beijing Cewei Photoelectricity Technology Co. Ltd) equipped with a high-speed camera (20 MP, USB 3.0). The generated emulsion droplets from the microfluidic device were carefully collected into a PTFE petri dish, which was subsequently placed into an oven to evaporate the solvent (water) at a setting temperature of 70 ℃. This solvent evaporation process lasted for 12 h and SiO_2 NPs-based superballs were obtained. The superballs were washed with *n*-hexane at least three times to remove any silicone oil residue. Afterwards, the superstructures were calcinated at 800 °C in a muffle furnace for 3 h and the SiO_2 photonic crystal microobjects with enhanced mechanical property were obtained. The microobjects after calcination were then immersed in aqua regia for 6 h to remove any impurities on the surface of the microobjects. Finally, the product treated with aqua regia was washed with deionized water three times. After the cleaning steps, the product was stored in deionized water for further use.

2.5. Preparation of hydrogel photonic microspheres with fully Inverse-Opal and partial Inverse-Opal structures

Hydrogel photonic crystal microspheres with full inverse-opal structure were prepared using the abovementioned SiO_2 NPs-based microobjects as templates. Firstly, 2.0 g acrylamide, 0.2 g acrylic acid, 0.1 g Bis-acrylamide and 2.0 μL DEAP photoinitiator were dissolved in 10 mL of deionized water. Secondly, the SiO_2 NP-based microspheres were immersed in this solution for 1 h to infiltrate the monomer solution into the voids among the SiO_2 NPs of the microballs. The monomer-filled SiO_2 microballs were subsequently placed in a home-made container, which was constructed by two glass glides with a spacing of 500 μm. Subsequently, the microspheres were irradiated with UV light for 40 min to polymerize the monomers, and consequently a hydrogel thin film embedded with SiO_2 NPs were obtained. The hydrogel film was subsequently transferred to deionized water to expand the hydrogel skeleton, and the SiO_2 NPs and hydrogel based composite photonic microspheres were separated from the hydrogel film by mechanical stripping. The composite microspheres were placed in 10 % HF solution for 2 h to completely etch the SiO_2 NPs. After the etching process, the resulting microobjects were washed with deionized water three times. Therefore, hydrogel photonic microobjects with fully inverse-opal structures were obtained. The fully inverse-opal photonic microobjects were stored in deionized water for property tests and structural characterizations. To obtain photonic microobjects with partial inverse-opal structure, the SiO_2 NPs/hydrogel hybrid microballs were immersed in a 10 % HF solution to initiate the etching of SiO_2 NPs. Unlike just simply waiting for the complete etching of the SiO_2 NPs, the microballs were picked out at any given moment, such as after 1 min of etching etc., and placed into a container with a large amount of distilled water to quench the etching reaction, leaving a portion of unreacted SiO_2 NPs remaining in the microballs. This action allows the etching process to be quenched at any given moment. Therefore, photonic microobjects with a partially etched inverse-opal structure can be obtained.

2.6. Characterization of SiO_2 NPs and photonic microobjects

Diluted drops of each batch of synthesized SiO_2 NPs were cast on silicon wafers (0.5 cm × 0.5 cm) and air-dried at room temperature. The dried samples were characterized under a Scanning Electron Microscope (FEI) with an accelerating voltage of 10 kV. To characterize the photonic properties of the photonic microobjects, the corresponding samples were placed under an inverted optical microscope (Olympus BX53M) that was equipped with a fiber spectrometer (Ocean Insight, Flame-*T*-UV–VIS Spectrometer). The etching process was also monitored using the same microscope equipped with a high-speed camera (Olympus DP74).

2.7. Synthesis and characterization of Ruthenium-Functionalized positively charged polymer PNIPAAm-co-Ru(bpy)$_3$

The synthesis of positively charged linear polymer PNIPAAm-*co*-Ru $(bpy)_3$ was achieved through a standard radical polymerization process similar to previous reports [56,57]. Briefly, 5.00 g monomer *N*-isopropyl acrylamide (NIPAAm), 0.5 g monomer $Ru(bpy)_3$ were placed in a 100 mL three-neck flask and dissolved in a mixture solution (50 mL) of acetone and water (volume ratio 1:9). The flask was equipped with a thermometer and a condenser. The solution was degassed with N_2 purging for at least 30 min. Subsequently, the solution was heated to 70 ℃ under N_2 protection. This condition was maintained for another half an hour and subsequently, 0.03 g KPS in 2 mL distilled water was dropwise added to the reaction flask to initiate the polymerization reaction, which was maintained for another 6 h at 70 ℃ under N_2 protection. Afterwards, the product solution was cooled down and transferred to a dialysis tube for dialysis. The dialysis process lasted for at least two weeks with frequent water changes. Finally, the purified product was freeze-dried and stored under cool and dry conditions for further use. A solution of the product at a concentration of 8 mg/mL was prepared for ^{1}H NMR characterization and the solvent was d^6-DMSO.

2.8. Modification of the photonic microcapsules with Ruthenium complex compound and Ruthenium-Functionalized linear polymer pNIPAAm-co-Ru (bpy)$_3$

The functionalization of the photonic microobject is achieved by a straightforward method. Given that the skeleton of the photonic microobject is PAAm-*co*-AAc polymer, where multiple pendant AAc groups are covalently attached to the skeleton of the microobject. The negatively charged polymer skeleton can further react with positively charged Ruthenium related compounds, such as Tris(bipyridine)ruthenium (II) chloride or Ruthenium-functionalized polymer PNIPAAm-*co*-$Ru(bpy)_3$. For the functionalization with small molecular-based Ruthenium compounds, the photonic microobjects were transferred from pure water to the small molecular-based Ruthenium compound solution (0.5 wt%) and kept in the solution for 24 h. This allows the small molecules to react with the polymer skeleton of the photonic microobjects sufficiently. Afterwards, the photonic microobjects were taken out and washed with pure water for several times. For the polymer functionalization experiments, the photonic microobjects were reacted with the Ruthenium-functionalized polymer solution for at least 24 h and subsequently transferred to a dialysis tube. The products were dialysis against pure water for at least 24 h with excess amount of water and frequent water change to remove the residues.

2.9. Preparation of the photonic microobjects embedded hydrogel film for anticounterfeiting performance test

Sodium alginate (2.5 wt%) solution was used to obtain a sodium alginate hydrogel film by shaping it in calcium chloride solution (1 wt %); Different matrix solutions were used as the matrix materials for embedding the ruthenium-functionalized photonic microobjects. These

solutions include an aqueous solution of the mixture of OEGMA and PEGDA (OEGMA and PEGDA mole ratio 100:7, water 20 wt% of monomer), PEGPEA, aqueous solution of OEGMA (20 wt%), aqueous solution of $PEGDA_{600}$ (20 wt%), a mixed solution of acrylamide and acrylic acid (2.0 g acrylamide, 0.2 g acrylic acid, 0.1 g crosslinker Bis-acrylamide). The polymer hydrogel film made of PEGDA600 and OEGMA, polymerized PEGPEA film, polymerized PEGDA600 film, and polyacrylamide hydrogel film were respectively obtained by photo-polymerizing the pregel solutions. Within each polymer film, at least one photonic microcapsule was embedded to test their appearance and screen materials for the construction of the polymer film. After the screening process, an optimal material's recipe was selected for further construction of the polymer film.

Specifically, a group of the photonic microobjects were placed in a glass slide mold with a round cavity (5 × 5 × 0.8 mm, Lianyungang Xiaoye Optoelectronics Technology Co.) A certain amount of the as-prepared matrix solution (these solutions include an aqueous solution of the mixture of OEGMA and PEGDA, PEGPEA, aqueous solution of OEGMA, aqueous solution of $PEGDA_{600}$, a mixture solution of acrylamide and acrylic acid) was carefully added to fill the mold. Then, a UV lamp (Jiapeng ZF-5, Shanghai, China, 365 nm, 16 W) was placed over the mold to initiate curing of the matrix material. Afterwards, a hydrogel film with the photonic microobjects embedded can be formed after at least 1 min of UV light irradiation. The resulting hydrogel film was carefully peeled off for further characterizations.

3. Results and discussion

3.1. Preparation of the photonic microobjects

The fabrication of colloidal photonic microobjects is achieved by a multiple-step procedure. Scheme 1 illustrates the fabrication of the photonic microobjects. An aqueous dispersion of monodispersed SiO_2 NPs was emulsified by a silicone oil solution in a microfluidic device. The carefully collected droplets were steadily standing on the surface of the PTFE petri dish. Due to the superhydrophobic property of the petri dish, the droplets were able to maintain a spherical shape [35] Although covered with the silicone oil solution, the droplets started to experience water evaporation. Simultaneously, due to the monodispersed size feature, the SiO_2 NPs within the droplets underwent a self-assembly process and organized into a close-packed ordered opal structure [58]. The formation mechanism of the opal structure was the same as that of a previous report [59]. The voids among SiO_2 NPs within the microparticles were filled with monomer solution after immersion of the SiO_2 NPs-based supraparticles in the aqueous solution of monomers for at least 4 h. This allowed the monomer solution to sufficiently fill the voids among SiO_2 NPs. Once the monomer solution-filled microobjects together with the monomer solution were placed in a home-made glass slide spacer container, the solution was immediately irradiated with UV light to initiate the monomer's polymerization. Therefore, the microballs were embedded in the pAAm-*co*-AAc hydrogel film and transformed into SiO_2 NPs-hydrogel composite microobjects. To ensure sufficient polymerization of monomers inside the microballs, a relatively long period of UV irradiation, such as 30 min in our case, was applied in our experiment. Afterwards, the microballs were separated from the hydrogel matrix by carefully mechanical stripping. The obtained hybrid photonic microballs were subsequently transferred to an HF solution for wet etching. The photonic microobjects that are partially etched by the HF solution can be further functionalized with positively charged linear polymers, such as pNIPAAm-*co*-$Ru(bpy)_3$. The entire process for the construction of the photonic microobjects is illustrated in Scheme 1.

3.2. Preparation of Opal-Structured and fully inverse Opal-Structured photonic microballs

Fig. 1 shows the generation of droplets and the formation of opal-structured photonic microballs. Fig. 1a shows the optical microscopy (OM) image of droplets inside the microfluidic channel. Fig. 1b and c show the OM image of the droplets with uniform diameter ~ 500 μm after collecting and photograph of the droplets sitting on the surface of a PTFE petri dish. Fig. 1d represents a green color composite photonic microsphere. SEM images in Fig. 1e–f clearly reveal that the microball is constructed with periodic organized monodispersed SiO_2 NPs. The microball was cut into two halves and the cross-section was characterized under SEM. Fig. 1g shows the SEM image of the cross-section of the microball. The image clearly reveals that inside part of the microball was also filled with periodically organized SiO_2 NPs. The green hexagons in Fig. 1f–g indicate that the SiO_2 NPs self-organized into perfect hexagonal structures both on the surface and inside of the microball. To obtain hydrogel inverse-opal photonic microball, the opal structure microball was immersed into a HF solution (10 wt%) and wet etching of SiO_2 NPs started to take place. The etching reaction lasted at least 2 h. After the etching and subsequent washing steps, the product was characterized under optical microscope again. The initially green opal microsphere was transformed into a pink color with fully inverse-opal structure (Fig. 1h). The corresponding reflection spectra in Fig. 1**i** further verifies the photonic property change before and after the wet etching process. Specifically, the microball before etching shows a maximum reflection wavelength at ~ 530 nm, while this value dramatically red shifts to 623 nm after the etching process. This phenomenon can be explained from two aspects: on the one hand, the polymer skeleton was constrained within the close-packed SiO_2 NPs of the microball prior to wet etching,

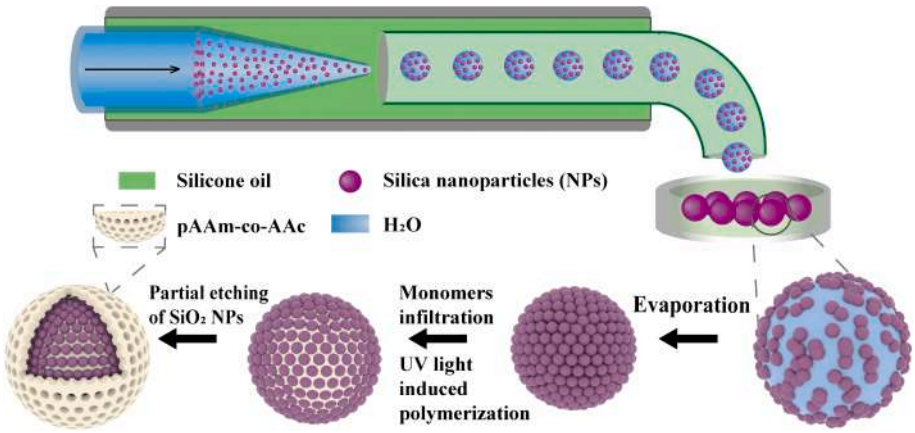

Scheme 1. Illustration shows the fabrication of photonic microobjects with full inverse opal and partial inverse opal structures via complete etching and controlled etching processes.

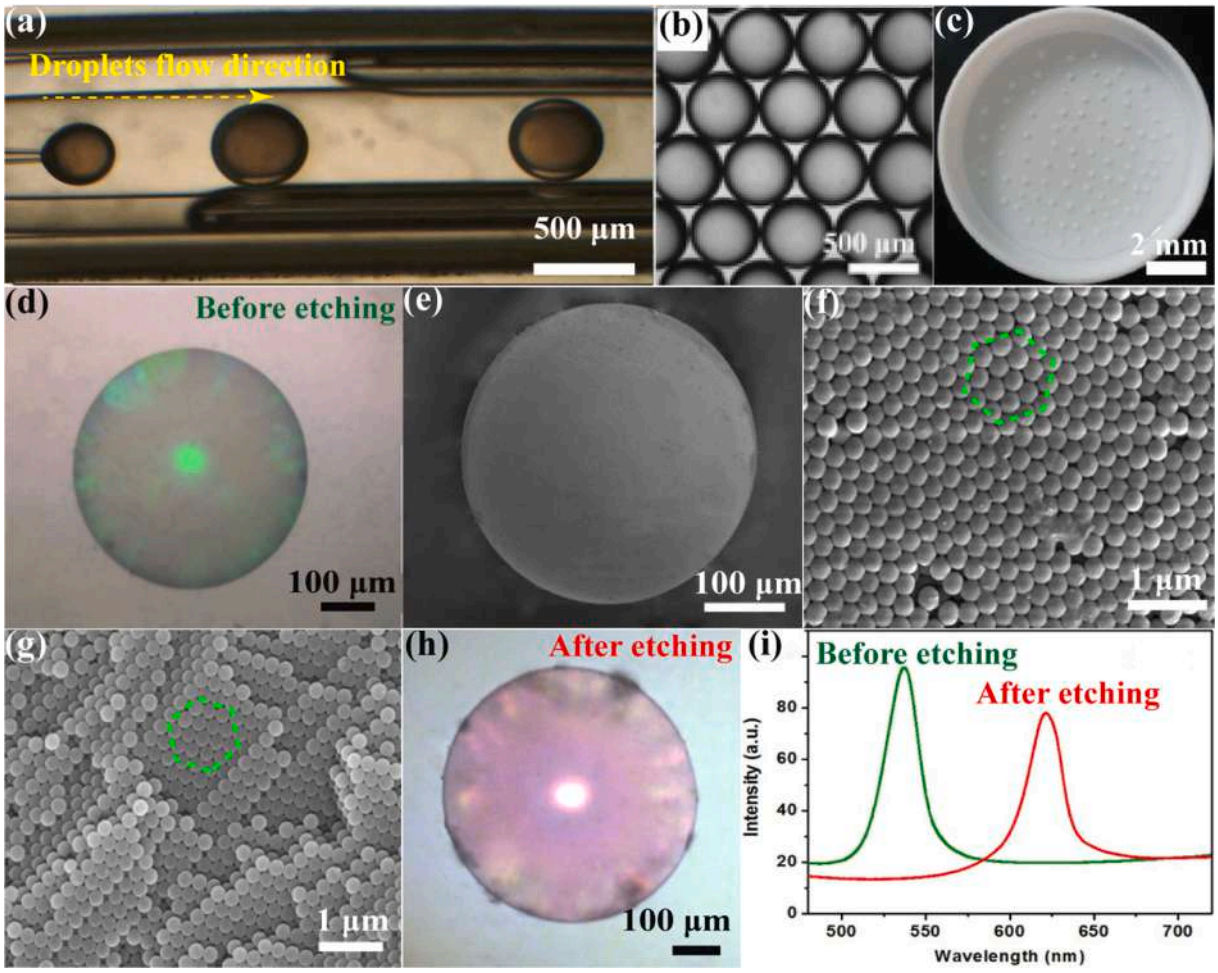

Fig. 1. Droplets generation process and the characterizations of the subsequent photonic microobjects evolved from the droplet templates. (a-b) OM images of droplets of SiO_2 dispersion generation in a glass capillary microfluidic device (a). and the collected droplets (b). (c) Photograpgh the droplets collected in a PTFE petri dish. (d) OM image of a green color SiO_2 NPs-hydrogel composite microball. (e) SEM image of an opal photonic microball constructed by SiO_2 NPs. (f) Enlarged SEM image of the surface of the microball, the green hexagon shows the hexagonal structure from SiO_2 NPs. (g) Cross-sectional SEM image of the microball. (h) OM image (Reflection mode) of a hydrogel photonic microball with inverse opal structure. (i) Reflection spectra of the photonic microball before (green curve) and after(red) HF etching. (For interpretation of the references to color in this figure legend, the reader is referred to the web version of this article.)

so the photonic property of the opal structure microball was utterly depending the close-packed SiO_2 NPs; on the other hand, after the wet etching, the constraint was removed due to the dissolution of the SiO_2 NPs. Moreover, the polymer hydrogel skeleton can absorb a large amount of water and induce a size expansion from ~ 440.50 μm (Fig. 1**d**) to ~ 530.06 μm (Fig. 1h) after the purification and re-dispersion of the inverse-opal microball into water. The synergistic effect resulted in the red-shift of the photonic microobject.

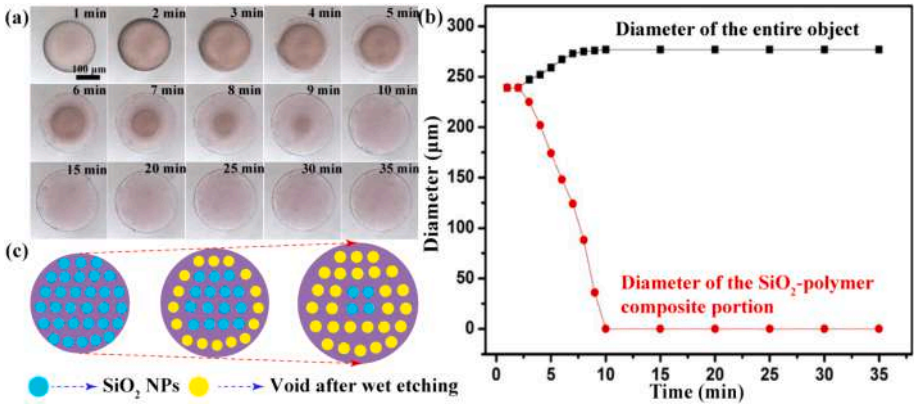

Fig. 2. (a) OM images of the SiO_2 NPs-polymer hydrogel composite microball evolves in 10 wt% HF solution. (b) Diameters of the entire object and the SiO_2-polymers composite part change as a function of time. (c) Schematic illustration of the evolution of the microball in the HF solution.

3.3. Monitoring the etching process under optical microscopy

To track the wet-etching process, a SiO_2 NPs/pAAm-*co*-AAc composite photonic microball was put into a 5 % HF solution and the sample was placed under an OM for real-time monitoring. Fig. 2 shows the evolution of the microball with an initial diameter of ~ 240 μm in the HF solution. OM images of the microball in Fig. 2a clearly demonstrate the change of the microball with time. The optically homogeneous microball shows no obvious change in the first two minutes in the HF solution, either from the point view of size or in terms of morphology. While after 3 min, morphology change of the microball starts to emerge, the initially homogeneous structure gradually transformed into a core–shell structure with the core and shell parts respectively having different optical contrasts: the darker SiO_2 NPs-hydrogel composite core and the brighter hydrogel shell part. This can be ascribed to the higher refractive index of SiO_2 NPs (~1.475) over that of the hydrogel polymer network (~1.33) [60]. The shell portion increases with time increase, while the core part simultaneously declines. Meanwhile, the size of the entire object increased due to the increased portion of the initially constrained hydrogel network was free from the dissolution of close-packed SiO_2 NPs. The darker core part completely disappeared after 10 min of dissolution in HF solution and then the morphology kept unchanged, indicating that the wet etching of SiO_2 NPs completed in a matter of 10 min. Meanwhile, the diameter of the entire object gradually increased with the etching reaction proceeds and kept at a constant value of ~ 280 μm after 10 min (the black dash curve in the Fig. 2b), revealing that the remaining neat hydrogel skeleton reached the maximum swelling capability after 10 min of etching. Conversely, the diameter of the SiO_2 NPs-polymer composite part decreased with time increase, particularly this portion was completely disappeared after 10 min, yielding neat polymer hydrogel network. Fig. 2c depicts the evolution of the microobject in the HF solution.

3.4. Preparation of Partial-Etched colloidal photonic microobjects

To take advantage of the etching reaction and generate photonic structure with more complex structure, we took actions to intervene in the middle of the reaction rather than waiting for the completion of the etching reaction. Specifically, the microball was taken out from the HF solution at any moment before the completion of the etching and immediately transferred into an excess amount of pure water to quench the etching reaction. Subsequently, a partial etched photonic microobject showing complex photonic property can be obtained. In specific, the photonic microobject with dual stopbands and distinct colors in a quasi-core–shell fashion were achieved. Taking a SiO_2 NPs-hydrogel composite microobject with initial green color for example, Fig. 3 shows a comparison of the photonic microobject before and after 5 min of etching (The OM images of the etching process are shown in **Figure S3**). Fig. 3(a) and (c) illustrate the structure of an initial green photonic microball before and after 5 min of HF etching. Fig. 3(b) and (d) show the OM images (Reflection mode) of the initial green photonic microball before and after 5 min of HF etching. The refractive index (RI) changes (refractive index before the wet etching is the combinational RI of SiO_2 NPs and the hydrogel network while the refractive index after the wet etching is the RI of the hydrogel network, and the refractive index is calculated by Eq. (1) in **Figure S1**.) before and after the etching of the SiO_2 NPs facilitated us for the monitoring of the etching process simply under optical microscopy. Clearly, the initially homogeneous microball evolved into a microobject with a core/shell-like structure and distinct optical contrast between core and shell parts, as labeled by different colors of text in Fig. 3d. In particular, there was a region in between the core and shell parts, as circled by the two pink dashed circles in Fig. 3d, showing a different contrast from both the core and shell parts. Correspondingly, the microobject before and after 5 min of etching showed different photonic phenomenon under reflection mode of the optical microscope: the center part of the microobject showed a green color before etching while the shell part of the microobject turned pink after 5 min of etching. A blurred region that lied in between the core and shell parts was also observed, as labelled by the pink dashed circles in Fig. 3d. Interestingly, the reflection spectrum of the microobject diverged from an initial single peak at a value of 513 nm to three different peaks: two sharp peaks at 509 nm and 602 nm and a shoulder peak at 613 nm, respectively. The peak value at 509 nm was identified as the reflection originated from the inner most core part, while the peak values at 613 nm and 602 nm were likely due to the reflection spectra from the shell part and the transition region between core and shell part, respectively (The similar phenomenon was also observed in a different microobject, as shown in **Figure S5**). There was a slight blue shift (4 nm) for the peak in the center region of the microobject. This was probably due to the experimental error.

Since the polymer skeleton is the pAAm-*co*-AAc based hydrogel, which is a well-known pH responsive polymer and has been widely

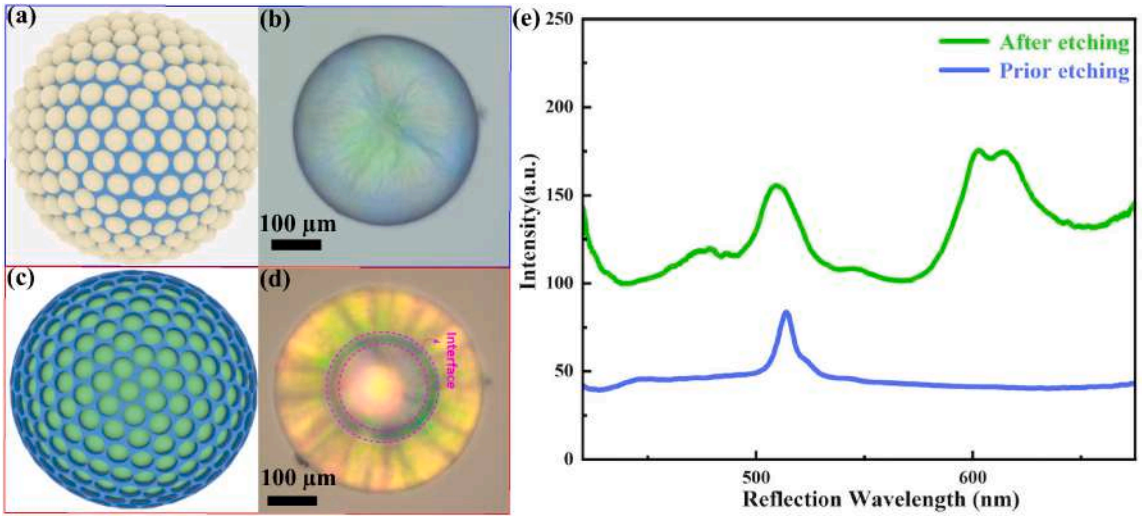

Fig. 3. (a) Schematic illustration of SiO_2 NPs-hydrogel composite microball. (b) Corresponding OM image (reflection mode). (c) Schematic illustration of partially etched SiO_2 NPs-hydrogel composite photonic microball. (d) Corresponding OM image (reflection mode). (e) Reflection spectra of the initial green photonic microobject (corresponding to b) before and after 5 min of etching (corresponding to d). (For interpretation of the references to color in this figure legend, the reader is referred to the web version of this article.)

explored in the field of sensing due to their stimulus responsive property.[61].However, our photonic microobject is featured with dual stopbands, where the outer shell is the neat hydrogel skeleton and the inner core part is composed of the polymer skeleton and SiO_2 NPs. The polymer close to the core part was constrained in the voids among SiO_2 NPs and likely their stimulus-responsive property was deactivated. In order to verify this hypothesis, a photonic microcapsule was placed into aqueous solutions of different concentrations of ethanol. The photonic performance of the microobject is shown in Fig. 4. The initial microobject displayed two distinct colors, where the core and shell parts displaying vivid green and red color, respectively. Correspondingly, the reflection spectrum peaks of the microcapsule with values were located at 537 nm and 703 nm, respectively, when the microcapsule was immersed in pure water (Fig. 4a). With the concentration of ambient ethanol solution increased from 0 to 60 wt%, the initially green-core/red-shell microcapsule displayed distinct color change trends in terms of the core and shell parts: the vivid green color kepte almost unchanged while the red color from the shell part displayed remarkable color change from red to purple (Fig. 4b–g). This phenomenon was consistent with the reflection spectrum measurements. Correspondingly, the reflection spectra from the two parts displayed completely different behaviors: the peak value at 537 nm remains unchanged (except in the case of 30 wt% of ethanol solution, where there was an overlapping effect of the two initial separate reflection peaks) in terms of the position. However, the peak value at 703 nm from the shell region gradually shifted to ~ 481 nm, more than 200 nm of reflection spectra peak value shifting (Fig. 4i–j and another example of a different photonic microobject as shown in **Figure S6**). These phenomena can be ascribed to two reasons: on the one hand, the pAAm-*co*-AAc skeleton in the core part was constrained at the voids among the SiO_2 NPs and consequently the polymer chain losses its stimulus responsive property; on the other hand, the polymer skeleton in the shell region was free to change configurations to adapt the stimuli of ethanol solutions. As a result, the polymer in the shell region gradually changed from swollen to shrunk status as the ethanol concentration increased, while the polymer skeleton in the core region was constrained. As a consequence, the entire microcapsule displays size decreased from ~ 497 μm to 376 μm while the diameter of the core part remains unchanged at ~ 249 μm in the entire process (Fig. 4j). In addition to the peak position change, the peak intensity change phenomenon was also accompanied by the entire process. This change was likely due to two aspects of synergistic effect: the hydrogel portion was in highly swollen state in neat water while the swollen state gradually switched to shrunk state and induced an increase in the refractive index. In our case, assuming the porous gel keeps the fine structure of the

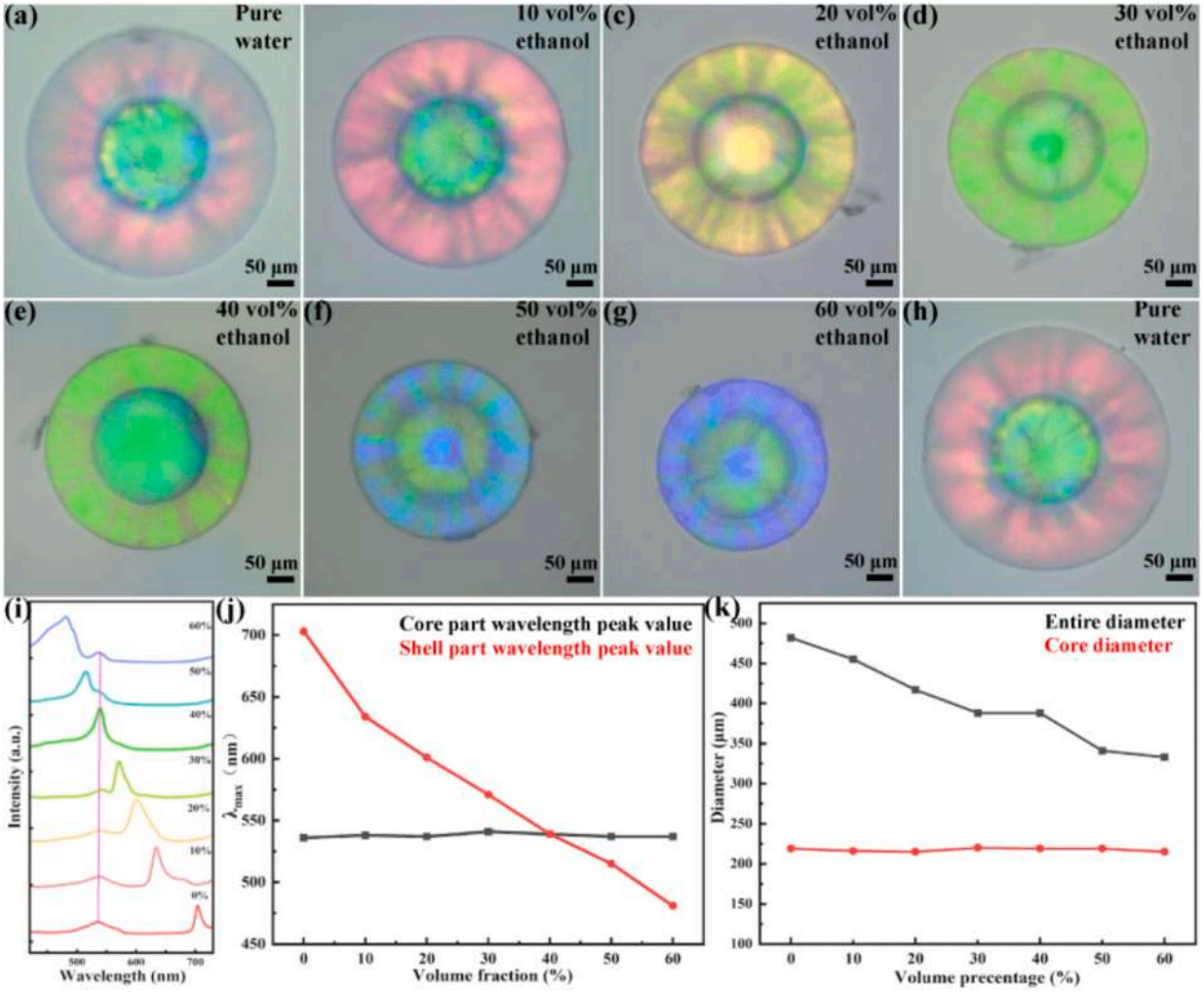

Fig. 4. Responsive behavior of a SiO_2 NPs-hydrogel composite microobject with a quasi core–shell (green core-red shell) structure to different concentrations of ethanol solution. (a-h) OM images of the microcapsule in different concentrations (v/v) of ethanol solutions from 0 to 60% (a-g) and back to 0% (h) again. (i) Reflection spectra change of the microcapsule in different concentrations of ethanol solutions. (j) Peak values of the reflection spectra of the microcapsule change in different concentrations of ethanol solutions from 0 to 60%. (k) Diameter changes of the core part and entire microcapsule in different concentrations of ethanol solutions. (For interpretation of the references to color in this figure legend, the reader is referred to the web version of this article.)

precursor colloidal crystal and the volume change was isotropic, the maximum reflection spectrum value from the (1 1 1) planes of the porous gel can be expressed by the modified Bragg Equation as below:

$$\lambda_{max} = 1.633(d/m)(l/l_0)(n_{av}^2 - sin^2\theta) \quad (1)$$

where d and m are the diameter of colloidal particles and the order of the Bragg diffraction, respectively. l and l_0 represent the thickness of the porous shell region of the microcapsules in the equilibrium state of certain conditions and in the as-prepared state, respectively. n_{av} is the average refractive index of the porous gel region by considering both the volume fraction of the gel portion and the voids under certain conditions. θ is the angle measured from normal to the gel surface at a specific point.

In our particular case, n is the refractive index of the pure polymer hydrogel region, d and θ are the lattice distance and angle of the incident light. Here θ is considered as a constant value of 90° given the incident light is vertical towards the photonic microobject. Meanwhile, n and d respectively increases and decreases with the shrinkage of the polymer skeleton, yielding the decrease of maximum reflection spectrum peak value, corresponding to the blue shift of the phenomenon. Furthermore, we carried out the experiments by repeatedly changing the concentrations of ethanol in the incubation solutions to test the reversibility of the microcapsules. Experimental results indicated that the localized ethanol responsive behaviors can repeat at least five times in our observations. The variations of the maximum peak values and minimum peak values of the reflectance spectra during cycling were only ~ 1 %, and the variations of the microcapsule at maximum diameter and minimum diameters were both only ~ 2 %. The maximum and minimum reflection spectrum wavelength values change and the diameter changes of the entire photonic microcapsule change during the repeating cycles are shown in Figure S11.

3.5. Functionalization of the Partial-Etched photonic microobjects

To introduce more functionalities to the resulting photonic

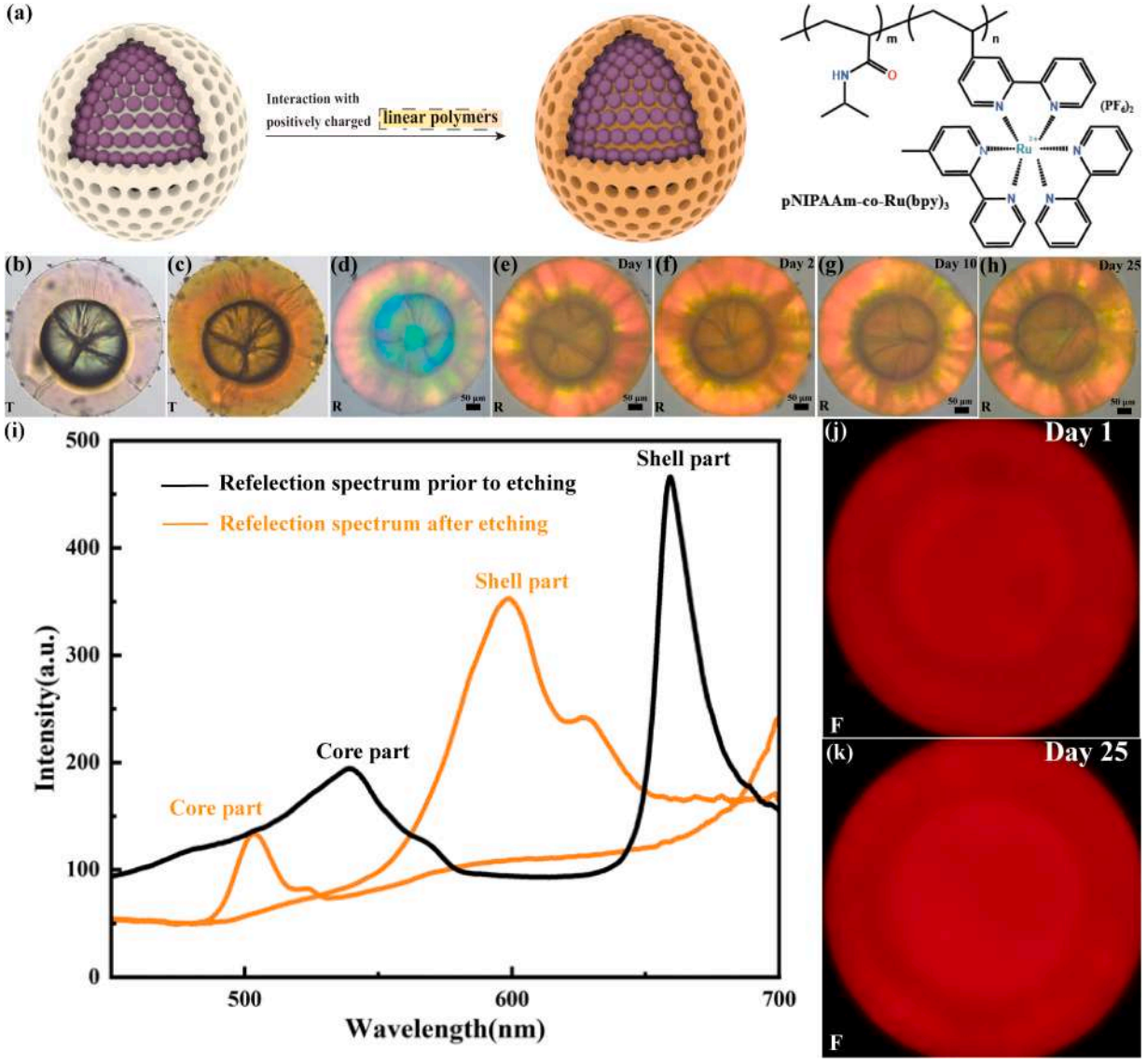

Fig. 5. (a) Schematic illustration of the formation of Ruthenium-functionalized core–shell photonic microobject through the interaction between positively charged linear polymers with the negatively charged polymer skeleton on the photonic microobject (left). Chemical structure of the Ruthenium-functionalized linear polymer (right). (b and c) OM images (transmission mode) of a photonic microobject before and after reaction with the Ruthenium-functionalized linear polymer. (d-h) OM images (reflection mode) of the photonic microobject before and after reacting with the Ruthenium-functionalized linear polymers and incubation in distilled water for different periods. (i) Reflection spectra of the photonic microobject before and after the ruthenium-functionalized polymer's labelling. (j-k) Fluorescence microscopy images of the Ruthenium-functionalized photonic microobject after day 1st and day 25th in distilled water.

microobjects, it is highly desirable to integrate more compositions into the individual photonic microobject. Fluorescent compositions, including QDs are normally selected as components to decorate photonic microobjects with fluorescent properties. However, this route normally requires the synthesis of core–shell colloidal particles (i.e., QDs as the core and PMMA or PS as the shell part) and subsequently use those colloidal particles as building blocks for the construction of photonic structures or through the co-assembly of QDs with ordinary colloidal particles to form binary photonic structures [62–64]. The two approaches more or less have their own disadvantages, either complicating the fabrication process or may introduce photonic defects into the photonic structures. In our case, we could introduce the fluorescent composition in a straightforward manner simply by leveraging the electrostatic interaction between a positively charged Ruthenium-functionalized linear polymer and the negatively charged pAAm-*co*-AAc skeleton. The reactions between polymers provided multiple binding sites and endowed the polymers with the capability to stick to the photonic microobjects in a stable fashion. Specifically, the multiple acrylic acid groups in the polymer skeleton of the photonic microobject can react with the Ruthenium-functionalized linear polymer and decorate the photonic microobject with fluorescent properties (Fig. 5**a**). The photonic microobjects modified with the Ruthenium-functionalized linear polymer (chemical structure as shown in Fig. 5**a** right panel and characterizations are shown in **Figure S8-9**) displayed a certain degree of swelling. For example, for the partially and fully etched microobjects, the swelling degrees were 3.1 % and 9.3 % (**Figure S10**), respectively. Moreover, the Ruthenium-functionalized linear polymer in water also exhibited an orange color, which could decorate the resulting photonic microobject with characteristic orange color under visual inspection or optical microscopy observation due to the MLCT effect (Fig. 5b–c of the transmission OM images).[65] And this orange color dominates the entire photonic microobject under visual inspection. Correspondingly, the photonic microobject before and after labelling with the Ruthenium-based polymer showed different phenomena under reflection mode characterization. Particularly, the photonic microobject initially showed a light green core and red shell, but it turned to dark green and orange after labelling (Fig. 5d–e). This phenomenon indicated that there was a color change of the photonic microobject towards the blue color direction after the polymer's complexation with the photonic microobject. The color change was further confirmed by the blue shift of the maximum reflection spectra of the photonic microobject (Fig. 5i). Specifically, the peak values of the reflection spectrum of the core and shell parts shifted from 547 nm and 660 nm (the black curve in Fig. 5i) to 501 nm and 598 nm (the orange curves in Fig. 5i), respectively. Considering the photonic microobject after the labelling with Ruthenium-functionalized polymer showing 3.1 % of diameter increase (**Figure S10**), which should induce the increase of the lattice distance and consequently red shift of the structural color. However, the observed color change is blue-shifting, suggesting the color shift is due to some other factors, such as the color mixing effects. In addition, the photonic microobjects were also featured with fluorescent property due to the incorporating of the Ruthenium-functionalized polymers (Fig. 5j–k). The Ruthenium-functionalized polymers were resistant to detaching from the polymer skeleton of the photonic microobject, indicating the electrostatic interaction was strong enough to keep the polymers on the skeleton of the photonic microobjects stable. Comparably, photonic microobjects modified with a low molecular weight Ruthenium-containing complex compound (Tris (2,2-Bipyridyl) Ruthenium (II) Chloride Hexahydrate) were less stable than the photonic microobjects modified with Ruthenium-based polymers (**Figure S7**). This phenomenon can be verified by the different time frames of the photonic microobject from Fig. 5**e**–h, where the photonic microobject almost kept constant both in terms of the size change trend and the structural colors of the microobject under optical microscope observation after 10 days in distilled water (**Figure S10**).

3.6. Preparation of a hydrogel film containing Ruthenium-Functionalized photonic microobjects

Owing to the abovementioned features, the Ruthenium-functionalized photonic microobjects can be further used as building blocks for the construction of anticounterfeiting structures. To produce the ruthenium-functionalized microobjects, photonic microobjects with a uniform green core and red shell were used as the primary building blocks (Fig. 6a). The microobjects showed a light green core and orange shell after modification with the ruthenium-functionalized polymers (Fig. 6b). As a proof-of-concept, hydrogel film embedded with the ruthenium-functionalized photonic microobjects was fabricated using the mixture of OEGMA and PEGDA as the matrix material (Despite other different materials were also tested and used as the matrix materials for embedding the microcapsules, those materials more or less have their own shortcomings when compared with the hydrogel formed from the polymerization of OEGMA and PEGDA. More detailed information can be seen in **Figure S12**). The photonic microobjects in the films were tightly aligned and in a stable state, and the structural color representation was not affected. When the hydrogel film was inspected under an OM, different information can be viewed. For example, the individual photonic microobject under different modes provided different information when inspected with an OM. First, the individual photonic microobject showed a clearly marked core–shell structure under the transmission mode (Fig. 6c) but with an overall uniform yellow color. Secondly, when observed under the reflection mode, the individual photonic microobject showed a dark green core and orange shell structure, despite the orange color from the ruthenium moieties dominating the color appearances (Fig. 6b). These phenomena indicated that the hydrogel film at least possess two aspects of information. In addition, when the film was observed under the fluorescence mode, the entire photonic microobject showed a bright red fluorescence color (Fig. 6d), suggesting the film possessed a third aspect of information. Furthermore, the hydrogel film also showed different information from a visual point of view. Fig. 6e is the schematic diagram of the composite hydrogel film under a white light. The hydrogel film showed a clear orange characteristic color from the ruthenium moiety (Fig. 6**f**). Contrarily, the hydrogel film exhibited a clear red fluorescence color when irradiated with a UV light under dark field (as illustrated in Fig. 6g and shown in Fig. 6h). These macroscopic phenomena indicated the hydrogel film possesses another two aspects of information. Put all together, the hydrogel film at least possessed fivefold of anticounterfeiting properties. The multiple anticounterfeiting properties of the photonic microobjects may have potential applications for the design of anticounterfeiting materials. This method and the relevant procedures to construct such kind of anticounterfeiting structures can be easily extended to large scale production when the experimental parameters are precisely controlled. This method and the relevant procedures to construct such kind of anticounterfeiting structures can be easily extended to large scale production when the experimental parameters are precisely controlled.

4. Conclusions

In summary, we have successfully constructed photonic microobjects that integrated both opal and inverse opal structures into an individual microobject. To achieve the fabrication of such kind of photonic microobjects, uniform opal photonic microspheres using monodispersed SiO_2 NPs as the building blocks were first fabricated via droplet microfluidics. The microspheres were subsequently placed into an aqueous solution of monomers to fill the voids among SiO_2 NPs with photocurable monomers, including AAm and AAc. The monomers-filled microspheres and the monomers' solution were irradiated with UV light to turn the pure SiO_2 NPs-based photonic microspheres into SiO_2 NPs-hydrogel composite photonic microobjects. The composite photonic microobjects were subsequently placed into a HF solution to initiate

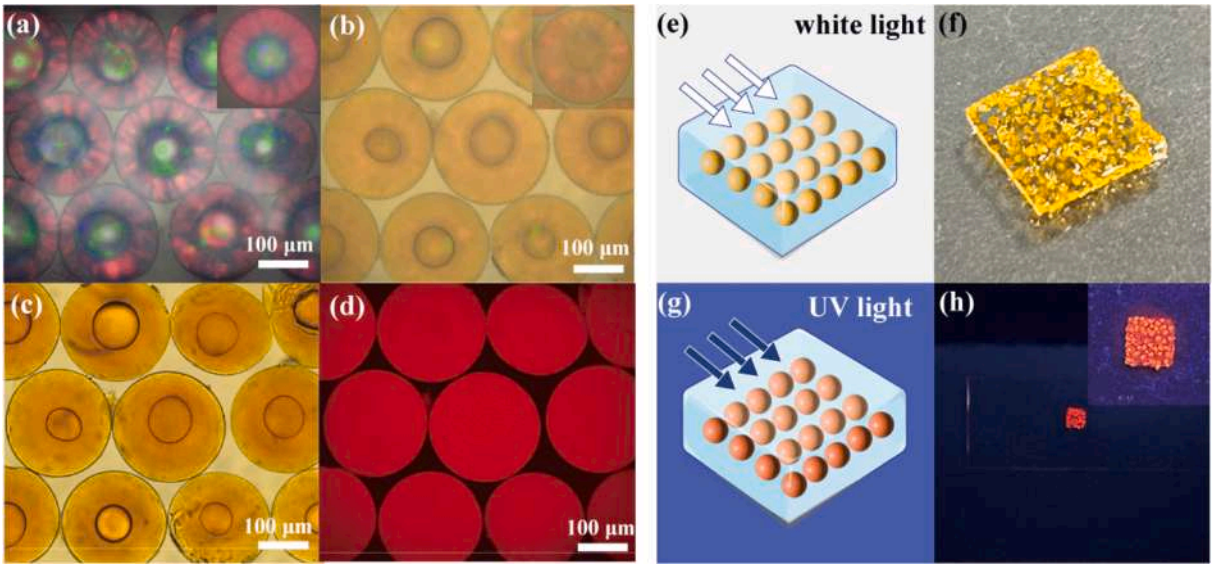

Fig. 6. (a) OM image of photonic microobjects before reacting with Ruthenium-functionalized linear polymer (reflection mode). (b and c) OM images of hydrogel film using ruthenium-functionalized photonic microobjects as the building blocks (reflection and transmission mode). (d) Corresponding fluorescence image. (e and f) Schematic illustration and photograph of the hydrogel film sample with photonic microobjects embedded under a white light. (g-h) Schematic illustration and photograph of the hydrogel film sample under a UV light irradiation.

etching of the SiO_2 NPs in a controlled manner, which can be achieved by quenching the etching reaction at any given moment. Through this operation, each individual photonic microobject integrating both opal and inverse opal structures was achieved. Therefore, the photonic microobjects featured with dual stopbands after the etching process. In addition, the photonic microobjects featured with reversible localized stimulus-responsive properties towards ethanol due to the partial inverse opal structure. Moreover, owing to the negatively charged feature of the polymer skeleton of the photonic microobjects, a positively charged linear polymer, pNIPAAm-*co*-Ru(bpy)$_3$, was readily attached to the skeleton of the photonic microobjects via the electrostatic interaction. The resulting photonic microobjects were featured with multiple properties, such as multiple photonic stopbands, fluorescence property and characteristic color from the Ruthenium moiety. The microobjects were further used as building blocks for the construction of hydrogel film, and these features endowed the hydrogel film with at least fivefold anticounterfeiting properties. We believe these photonic microobjects can be extended to other materials for different potential applications. This design opens a new route for the design of novel photonic microobjects and anticounterfeiting materials.

CRediT authorship contribution statement

Xiaoyang Du: Writing – original draft, Methodology, Investigation, Formal analysis, Data curation. **Chengnian Li:** Methodology, Investigation. **Jianying Wang:** Formal analysis. **Zhi Li:** Resources. **Jintao Zhu:** Writing – review & editing, Supervision, Resources. **Yajiang Yang:** Writing – review & editing, Supervision, Funding acquisition. **Yuandu Hu:** Writing – review & editing, Writing – original draft, Supervision, Project administration, Funding acquisition, Formal analysis, Conceptualization.

Declaration of competing interest

The authors declare that they have no known competing financial interests or personal relationships that could have appeared to influence the work reported in this paper.

Data availability

Data will be made available on request.

Acknowledgements

This work is supported by the Fundamental Research Funds for the Central Universities under the grant number KVJBMC23001536. Y. H. is also grateful for the open research fund support from the State Key Laboratory of Molecular Engineering of Polymers (Fudan University) under the fund number K2024-15.

Appendix A. Supplementary data

Supplementary data to this article can be found online at https://doi.org/10.1016/j.jcis.2024.05.108.

References

[1] H. Inan, M. Poyraz, F. Inci, M.A. Lifson, M. Baday, B.T. Cunningham, U. Demirci, Photonic crystals: emerging biosensors and their promise for point-of-care applications, Chem Soc Rev 46 (2) (2017) 366–388, https://doi.org/10.1039/c6cs00206d.
[2] J. Zi, X. Yu, Y. Li, X. Hu, C. Xu, X. Wang, X. Liu, R. Fu, Coloration strategies in peacock feathers, Proc. Natl. Acad. Sci. u.s.a. 100 (22) (2003) 12576–12578, https://doi.org/10.1073/pnas.2133313100.
[3] J. Teyssier, S.V. Saenko, D. van der Marel, M.C. Milinkovitch, Photonic crystals cause active colour change in chameleons, Nat. Commun. 6 (2015) 6368, https://doi.org/10.1038/ncomms7368.
[4] R.C. Thayer, F.I. Allen, N.H. Patel, Structural color in Junonia butterflies evolves by tuning scale lamina thickness, Elife 9 (2020), https://doi.org/10.7554/eLife.52187.
[5] W. Hong, Z. Yuan, X. Chen, Structural color materials for optical anticounterfeiting, Small 16 (16) (2020) e1907626, https://doi.org/10.1002/smll.201907626.
[6] J.V. Sanders, Colour of Precious Opals, Nature 204 (1964) 1151–1153.
[7] J.M. Weissman, H.B. Sunkara, A.S. Tse, S.A. Asher, Thermally switchable periodicities and diffraction from mesoscopically ordered materials, Science 274 (5289) (1996) 959–960, https://doi.org/10.1126/science.274.5289.959.
[8] Y. Kang, J.J. Walish, T. Gorishnyy, E.L. Thomas, Broad-wavelength-range chemically tunable block-copolymer photonic gels, Nat Mater 6 (12) (2007) 957–960, https://doi.org/10.1038/nmat2032.
[9] M. Vatankhah-Varnosfaderani, A.N. Keith, Y. Cong, H. Liang, M. Rosenthal, M. Sztucki, C. Clair, S. Magonov, D.A. Ivanov, A.V. Dobrynin, S.S. Sheiko, Chameleon-like elastomers with molecularly encoded strain-adaptive stiffening

and coloration, Science 359 (6383) (2018) 1509–1513, https://doi.org/10.1126/science.aar5308.
[10] G.M. Miyake, R.A. Weitekamp, V.A. Piunova, R.H. Grubbs, Synthesis of isocyanate-based brush block copolymers and their rapid self-assembly to infrared-reflecting photonic crystals, J. Am. Chem. Soc. 134 (34) (2012) 14249–14254, https://doi.org/10.1021/ja306430k.
[11] Q. He, K.H. Ku, H. Vijayamohanan, B.J. Kim, T.M. Swager, Switchable Full-Color Reflective Photonic Ellipsoidal Particles, J. Am. Chem. Soc. 142 (23) (2020) 10424–10430, https://doi.org/10.1021/jacs.0c02398.
[12] S. Valkama, H. Kosonen, J. Ruokolainen, T. Haatainen, M. Torkkeli, R. Serimaa, G. Ten Brinke, O. Ikkala, Self-assembled polymeric solid films with temperature-induced large and reversible photonic-bandgap switching, Nat Mater 3 (12) (2004) 872–876, https://doi.org/10.1038/nmat1254.
[13] K.G. Noh, S.Y. Park, Smart molecular-spring photonic droplets, Mater. Horizons 4 (4) (2017) 633–640, https://doi.org/10.1039/c7mh00155j.
[14] B.H. Miller, H. Liu, M. Kolle, Scalable optical manufacture of dynamic structural colour in stretchable materials, Nat Mater 21 (9) (2022) 1014–1018, https://doi.org/10.1038/s41563-022-01318-x.
[15] Z. Hu, G. Huang, A new route to crystalline hydrogels, guided by a phase diagram, Angew. Chem. Int. Ed. 42 (39) (2003) 4799–4802, https://doi.org/10.1002/anie.200351 326.
[16] H. Wang, Y. Liu, Z. Chen, L. Sun, Y. Zhao, Anisotropic structural color particles from colloidal phase separation, Sci Adv 6(2) (2020) eaay1438. https://doi.org/10.1126/sciadv.aay1438.
[17] M. Chen, L. Zhou, Y. Guan, Y. Zhang, Polymerized microgel colloidal crystals: photonic hydrogels with tunable band gaps and fast response rates, Angew Chem Int. Ed. 52 (38) (2013) 9961–9965, https://doi.org/10.1002/anie.201302466.
[18] J.P. Couturier, M. Sutterlin, A. Laschewsky, C. Hettrich, E. Wischerhoff, Responsive inverse opal hydrogels for the sensing of macromolecules, Angew. Chem. Int. Ed. 54 (22) (2015) 6641–6644, https://doi.org/10.1002/anie.201500674.
[19] S.H. Kim, S.J. Jeon, W.C. Jeong, H.S. Park, S.M. Yang, Optofluidic synthesis of electroresponsive photonic janus balls with isotropic structural colors, Adv. Mater. 20 (21) (2008) 4129–4134, https://doi.org/10.1002/adma.200801167.
[20] J.Y. Wang, Y. Cao, Y. Feng, F. Yin, J.P. Gao, Multiresponsive inverse-opal hydrogels, Adv. Mater. 19 (22) (2007) 3865–3871, https://doi.org/10.1002/adma.20060 2884.
[21] Q. He, Y. Cheng, Y. Deng, F. Wen, Y. Lai, H. Li, Conductive hydrogel for flexible bioelectronic device: Current Progress and Future Perspective, Adv. Funct. Mater. 34 (1) (2023) 2308974, https://doi.org/10.1002/adfm.202308974.
[22] M.A. Campea, M.J. Majcher, A. Lofts, T. Hoare, A review of design and fabrication methods for nanoparticle network hydrogels for biomedical, environmental, and industrial applications, Adv. Funct. Mater. 31 (33) (2021) 2102355, https://doi.org/10.1002/adfm.202102355.
[23] A.S. Utada, L.Y. Chu, A. Fernandez-Nieves, D.R. Link, C. Holtze, D.A. Weitz, Dripping, jetting, drops, and wetting: The magic of microfluidics, Mrs Bull 32 (9) (2007) 702–708, https://doi.org/10.1557/Mrs2007.145.
[24] S. Yang, Y.G. Kim, S. Park, S.H. Kim, Structural color mixing in microcapsules through exclusive crystallization of binary and ternary colloids, Adv. Mater. 35 (38) (2023) e2302750, https://doi.org/10.1002/adma.202302750.
[25] Z. Wang, R. Li, Y. Zhang, C.L.C. Chan, J.S. Haataja, K. Yu, R.M. Parker, S. Vignolini, Tuning the color of photonic glass pigments by thermal annealing, Adv. Mater 35 (34) (2023) e2207923, https://doi.org/10.1002/adma.202207923.
[26] M. Liu, J. Fu, S. Yang, Y. Wang, L. Jin, S.H. Nah, Y. Gao, Y. Ning, C.B. Murray, S. Yang, Janus microdroplets with tunable self-recoverable and switchable reflective structural colors, Adv. Mater 35 (5) (2023) e2207985, https://doi.org/10.1002/adma.202207985.
[27] J. Zhang, Y. Qin, Y. Ou, Y. Shen, B. Tang, X. Zhang, Z. Yu, Injectable granular hydrogels as colloidal assembly microreactors for customized structural colored objects, Angew. Chem. Int. Ed. 61 (34) (2022) e202206339, https://doi.org/10.1002/anie.202206339.
[28] J. Wang, C.F. Mbah, T. Przybilla, B. Apeleo Zubiri, E. Spiecker, M. Engel, N. Vogel, Magic number colloidal clusters as minimum free energy structures, Nat. Commun. 9 (1) (2018) 5259, https://doi.org/10.1038/s41467-018-07600-4.
[29] G. Liang, X. Zhu, Y. Xu, J. Li, S. Yang, Holographic design and fabrication of diamond symmetry photonic crystals via dual-beam quadruple exposure, Adv. Mater 22 (40) (2010) 4524–4529, https://doi.org/10.1002/adma.201001785.
[30] N. Vogel, S. Utech, G.T. England, T. Shirman, K.R. Phillips, N. Koay, I.B. Burgess, M. Kolle, D.A. Weitz, J. Aizenberg, Color from hierarchy: Diverse optical properties of micron-sized spherical colloidal assemblies, Proc. Natl. Acad. Sci. u.s.a. 112 (35) (2015) 10845–10850, https://doi.org/10.1073/pnas.1506272112.
[31] T. Kanai, D. Lee, H.C. Shum, R.K. Shah, D.A. Weitz, Gel-immobilized colloidal crystal shell with enhanced thermal sensitivity at photonic wavelengths, Adv. Mater 22 (44) (2010) 4998–5002, https://doi.org/10.1002/adma.201002055.
[32] X. Wu, R. Hong, J. Meng, R. Cheng, Z. Zhu, G. Wu, Q. Li, C.F. Wang, S. Chen, Hydrophobic Poly(tert-butyl acrylate) Photonic crystals towards robust energy-saving performance, Chem. Int. Ed. 58 (38) (2019) 13556–13564, https://doi.org/10.1002/anie.201907464.
[33] T.M. Choi, G.H. Lee, Y.S. Kim, J.G. Park, H. Hwang, S.H. Kim, Photonic microcapsules containing single-crystal colloidal arrays with optical anisotropy, Adv. Mater 31 (18) (2019) e1900693, https://doi.org/10.1002/adma.201900693.
[34] Y. Zhao, X. Zhao, J. Hu, M. Xu, W. Zhao, L. Sun, C. Zhu, H. Xu, Z. Gu, Encoded porous beads for label-free multiplex detection of tumor markers, Adv. Mater 21 (5) (2009) 569–572, https://doi.org/10.1002/adma.200802339.
[35] J. Wang, Y. Hu, R. Deng, R. Liang, W. Li, S. Liu, J. Zhu, Multiresponsive hydrogel photonic crystal microparticles with inverse-opal structure, Langmuir 29 (28) (2013) 8825–8834, https://doi.org/10.1021/la401540s.
[36] C.I. Aguirre, E. Reguera, A. Stein, Tunable colors in opals and inverse opal photonic crystals, Adv Funct Mater 20 (16) (2010) 2565–2578, https://doi.org/10.1002/adfm.201000143.
[37] G.I.N. Waterhouse, M.R. Waterland, Opal and inverse opal photonic crystals: fabrication and characterization, Polyhedron 26(2) (2007) 356-368. https://doi.org/10. 1016/j.poly.2006.06.024.
[38] P. Ni, P. Dong, B. Cheng, X. Li, D. Zhang, Synthetic SiO_2 opals, Adv. Mater 13 (6) (2001) 437–441, https://doi.org/10.1002/1521-4095(200103)13:6%3C437::AID-ADMA437%3E3.0.CO;2-8.
[39] N.A. Clark, A.J. Hurd, B.J. Ackerson, Single Colloidal Crystals, Nature 281 (5726) (1979) 57–60, https://doi.org/10.1038/281057a0.
[40] Z. Yu, C.F. Wang, L. Ling, L. Chen, S. Chen, Triphase microfluidic-directed self-assembly: anisotropic colloidal photonic crystal supraparticles and multicolor patterns made easy, Angew. Chem. Int. Ed. 51 (10) (2012) 2375–2378, https://doi.org/10.1002/anie. 201107126.
[41] Y. Zhao, H. Gu, Z. Xie, H.C. Shum, B. Wang, Z. Gu, Bioinspired multifunctional Janus particles for droplet manipulation, J. Am. Chem. Soc. 135 (1) (2013) 54–57, https://doi.org/10.1021/ja310389w.
[42] H. Li, J. Wang, F. Liu, Y. Song, R. Wang, Fluorescence enhancement by heterostructure colloidal photonic crystals with dual stopbands, J. Colloid Interface Sci. 356 (1) (2011) 63–68, https://doi.org/10.1016/j.jcis.2010.12.078.
[43] B. Gao, L. Tang, D. Zhang, Z. Xie, E. Su, H. Liu, Z. Gu, Transpiration-inspired fabrication of opal capillary with multiple heterostructures for multiplex aptamer-based fluorescent assays, ACS Appl Mater Interfaces 9 (38) (2017) 32577–32582, https://doi.org/10.1021/acsami.7b10143.
[44] S.K. Nam, J.B. Kim, S.H. Han, S.H. Kim, Photonic janus balls with controlled magnetic moment and density asymmetry, ACS Nano 14 (11) (2020) 15714–15722, https://doi.org/10.1021/acsnano.0c06672.
[45] M.Q. Xiao, J.J. Liu, Z.J. Chen, W.X. Liu, C.C. Zhang, Y.Y. Yu, C.R. Li, L. He, Magnetic assembly and manipulation of Janus photonic crystal supraparticles from a colloidal mixture of spheres and ellipsoids, J. Mater. Chem. C 9 (35) (2021) 11788–11793, https://doi.org/10.1039/d1tc01543e.
[46] J.H. Lee, G.H. Choi, K.J. Park, D. Kim, J. Park, S. Lee, H. Yi, P.J. Yoo, Dual-colour generation from layered colloidal photonic crystals harnessing “core hatching” in double emulsions, J. Mater. Chem. C 7 (23) (2019) 6924–6931, https://doi.org/10.1039/c9tc01055f.
[47] B. Ye, H. Ding, Y. Cheng, H. Gu, Y. Zhao, Z. Xie, Z. Gu, Photonic crystal microcapsules for label-free multiplex detection, Adv. Mater 26 (20) (2014) 3270–3274, https://doi.org/10.1002/adma.201305035.
[48] S.S. Liu, C.F. Wang, X.Q. Wang, J. Zhang, Y. Tian, S.N. Yin, S. Chen, Tunable Janus colloidal photonic crystal supraballs with dual photonic band gaps, J. Mater. Chem. C 2 (44) (2014) 9431–9438, https://doi.org/10.1039/c4tc01631a.
[49] K. Zhou, T. Tian, C. Wang, H. Zhao, N. Gao, H. Yin, P. Wang, B.J. Ravoo, G. Li, Multifunctional integrated compartment systems for incompatible cascade reactions based on onion-like photonic spheres, J. Am. Chem. Soc. 142 (49) (2020) 20605–20615, https://doi.org/10.1021/jacs.0c00513.
[50] L.-W. Hao, J.-D. Liu, Q. Li, R.-K. Qing, Y.-Y. He, J. Guo, G. Li, L. Zhu, C. Xu, S. Chen, Microfluidic-directed magnetic controlling supraballs with multi-responsive anisotropic photonic crystal structures, J Mater Sci Technol 81 (2021) 203–211, https://doi.org/10.1016/j.jmst.2020.11.063.
[51] X.-Q. Yu, X. Zhang, T. Qiu, H. Liu, J. Guo, Q. Li, Z. Zhang, S. Chen, Engineering particles for sensing applications via in-situ synthesizing carbon dots@SiO2 photonic crystals, Chem. Eng. J 465 (2023) 142851, https://doi.org/10.1016/j.cej.2023.142851.
[52] C. Xu, D. Yang, L. Luo, D. Ma, S. Huang, Dual-modal invisible photonic crystal prints from photo/water responsive photonic crystals, Adv. Photonics Res 2 (7) (2021) 2000197, https://doi.org/10.1002/adpr.202000197.
[53] Z. Fang, S. Keinan, L. Alibabaei, H. Luo, A. Ito, T.J. Meyer, Controlled electropolymerization of ruthenium(II) vinylbipyridyl complexes in mesoporous nanoparticle films of TiO_2, Angew. Chem. Int. Ed. 53 (19) (2014) 4872–4876, https://doi.org/10.1002/anie.201402309.
[54] Y. Hu, J. Pérez-Mercader, Controlled synthesis of uniform, micrometer-sized ruthenium-functionalized poly(N-Isopropylacrylamide) gel particles and their application to the catalysis of the Belousov-Zhabotinsky reaction, Macromol Rapid Commun 38 (3) (2017) 1600577, https://doi.org/10.1002/marc.2016005 77.
[55] K.D. Kim, H.T. Kim, Formation of silica nanoparticles by hydrolysis of TEOS using a mixed semi-batch/batch method, J Solgel Sci Technol 25 (3) (2002) 183–189, https://doi.org/10.1023/A:1020217105290.
[56] Y. Hu, J. Pérez-Mercader, Microfluidics-Assisted Synthesis of Cross-Linked Colloidosomes with Multisensitive Behaviors: A Potential Platform for Photo Memory Device and Blue-Light-Triggered Release Vehicle, ACS Appl. Nano Mater. 1 (7) (2018) 3346–3354, https://doi.org/10.1021/acsanm.8b00554.
[57] Y. Hu, J. Tresback, J. Pérez-Mercader, Preparation of ruthenium-functionalized microgels through the intermolecular crosslinking of two functionalized polymers within droplets and study of their chemical/ photo-active behaviors, Polym. Degrad. Stab. 181 (2020), https://doi.org/10.1016/j.polymdegradstab.2020.109345.
[58] Y. Zhao, X. Zhao, C. Sun, J. Li, R. Zhu, Z. Gu, Encoded silica colloidal crystal beads as supports for potential multiplex immunoassay, Anal Chem 80 (5) (2008) 1598–1605, https://doi.org/10.1021/ac702249a.
[59] J.V. Saners, Colour of precious opals, Nature 4964 (1964) 1151–1153, https://doi.org/10.1038/2041151a0.
[60] J.B. Kim, J.W. Kim, M. Kim, S.H. Kim, Dual-colored janus microspheres with photonic and plasmonic faces, Small 18 (21) (2022) e2201437, https://doi.org/10.1002/smll.202201437.

[61] J.H. Holtz, S.A. Asher, Polymerized colloidal crystal hydrogel films as intelligent chemical sensing materials, Nature 389 (6653) (1997) 829–832, https://doi.org/10.1038/39834.
[62] K. Liu, Y. Tian, Q. Li, X.-Y. Du, J. Zhang, C.-F. Wang, S. Chen, Microfluidic printing directing photonic crystal bead 2D code patterns, J. Mater. Chem. C 6 (9) (2018) 2336–2341, https://doi.org/10.1039/c7tc05355j.
[63] A.Q. Xie, J.Z. Guo, L.L. Zhu, S. Chen, Carbon dots promoted photonic crystal for optical information storage and sensing, Chem. Eng. J. 415 (2021) 128950. https://doi.org/ARTN 12895010.1016/j.cej.2021.128950.
[64] F. Bian, L. Sun, H. Chen, Y. Wang, L. Wang, L. Shang, Y. Zhao, Bioinspired Perovskite Nanocrystals-Integrated Photonic Crystal Microsphere Arrays for Information Security, Adv Sci 9 (9) (2022) e2105278, https://doi.org/10.1002/advs.202105278.
[65] N.H. Damrauer, G. Cerullo, A. Yeh, T.R. Boussie, C.V. Shank, J.K. McCusker, Femtosecond dynamics of excited-state evolution in [Ru(bpy) (3)](2+), Science 275 (5296) (1997) 54–57, https://doi.org/10.1126/science.275.5296.